第 43 卷 第 2 期/2023 年 1 月/光学学报 研究论文

光学学报

# 调节精度可配置的可变光衰减器研究

魏硕，陈陶*，谌静，孔梅梅，关建飞

南京邮电大学电子与光学工程学院、柔性电子(未来技术)学院，江苏 南京 210000

**摘要** 设计了一种调节精度可配置的可变光衰减器结构，通过流体恒压泵驱动薄膜弹起，将流体压力/压强调节转化为光纤微位移控制，实现对接光纤横向位错及光学衰减。使用多物理场耦合与三维时域有限差分的方法对结构模型进行分析，并利用精细加工技术实现了器件的制作。通过对薄膜厚度的选配，实现了光强耦合效率的精度可调配置。理论分析和实验结果表明，选用合适的膜厚得到本衰减器的插入损耗为 1.24 dB，可变衰减范围大于 60 dB，波长相关损耗小于 1 dB。当设定可变光衰减器的光衰减动态范围分别为 10 dB 和 40 dB 时，配置 0.5 mm 薄膜厚度的调节精度分别优于 0.04 dB 和 0.11 dB；当膜的厚度增加时，调节精度会更高。

**关键词** 光通信；可变光衰减器；横向位错；薄膜驱动；精度可配置

**中图分类号** TN761 **文献标志码** A **DOI**：10.3788/AOS221140

## 1 引 言

可变光衰减器(VOA)是光纤通信中波分复用(WDM)传输节点功率均衡、光放大器增益平坦化、复用点信道平衡和接收节点功率管理的关键元件[1-2]。WDM 网络的不断发展，要求 VOA 更简单、稳健、紧凑、功耗更低，使实现 VOA 的方法也不断推陈出新[3]。VOA 的常见类型有磁光型[4]、微机电系统(MEMS)[5-8]、液晶型[9]、波导型[10-11]、温控型[12]及光纤可调型[13-14]等。谢晓强等[15]设计了利用电磁驱动器改变输入、输出光纤之间径向偏移的 VOA，插入损耗小于 1 dB，动态范围约 35 dB。Li 等[16]在单模光纤的基础上利用声光模式耦合实现了精度为 0.5 dB、动态范围为 0.3 dB～22 dB 的 VOA。随着光纤技术的不断发展[17]，用光纤做成的器件得以普遍应用[18-20]。光纤 VOA 以其结构简单、插入损耗低、成本低、方便与其他光纤及波导结构对接等优点，得到应用广泛[21]。调节精度和衰减范围是 VOA 非常重要的参数，目前调节精度高且衰减范围大的产品很少，调节精度可配置且动态范围大的 VOA 的研究未见报道，本文在传统位错型光纤 VOA 的动态范围大等优势的基础上，实现精度可配置的功能。

提出一种光纤位错型 VOA，采用流体恒压驱动薄膜凸起使光纤产生微量机械位错，控制光纤耦合效率，实现光信号的可控衰减，将流体压力/压强调节转化为光纤微位移控制易于实现光纤类产品的微量位移精密控制，避免使用具有高昂成本的精密机械调节仪器。器件符合光网络对于衰减器的要求，可以在很大的衰减范围内工作，并具有低插入损耗和低的波长相关损耗(WDL)，还有结构紧凑、成本低及精度高等优点。依据 VOA 光功率调节曲线，选配不同的膜厚，从而实现 VOA 光衰减精度的可配置。

## 2 器件设计

所设计的器件如图 1 所示，包括底部容器、薄膜及膜上光纤承载结构。容器为聚乳酸树脂通过 3D 打印而成的方形槽结构，外、内尺寸分别为 26 mm×26 mm×15 mm 和 20 mm×20 mm×10 mm。流体使用 20 ℃的纯水，密度为 998.2 kg/m$^3$，恒压泵的出口通道通过直径为 2.5 mm 的流体入口与方形槽的内部储液结构相通。聚二甲基硅氧烷(PDMS)薄膜均匀贴敷在容器上表面，杨氏模数为 750 kPa，密度为 970 kg/m$^3$，泊松比为 0.49[22]。薄膜上放置的光纤承载平台包含 3 层，采用密度为 2200 kg/m$^3$的石英玻璃片制成。平台的底层为 19 mm×19 mm×0.2 mm 的薄片；中间层为长宽比底层略大的 V 型槽片，用于单模光纤的胶粘固定[23]；上层为玻璃压板，可以辅助稳定压住光纤。光纤采用 THORLABS 公司的 SMF-28 Ultra 未镀膜单模光纤，恒压泵采用微流体 OB1 MK3+压力泵，参数如表 1 所示。

**收稿日期**：2022-05-16；**修回日期**：2022-07-05；**录用日期**：2022-07-18；**网络首发日期**：2022-07-28

**基金项目**：国家自然科学基金(11974188，61905117)、中国博士后科学基金(2021T140339，2018M632345)、江苏省博士后科学基金(2021K617C)、南京邮电大学科研基金项目(NY220050)

**通信作者**：*chent@njupt.edu.cn

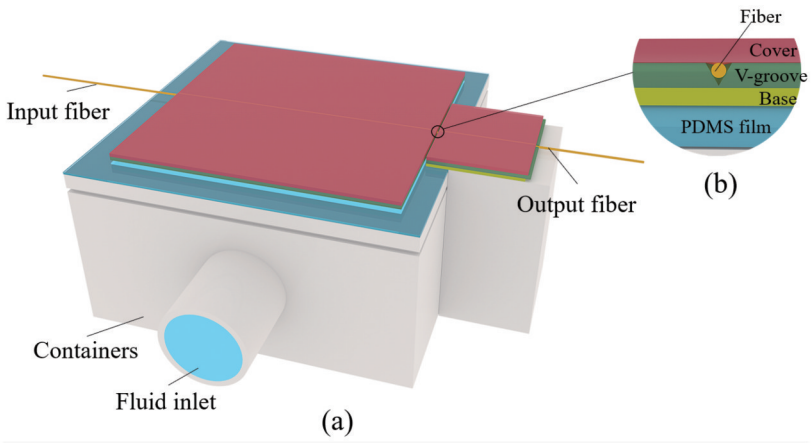


图 1　调节精度可配置的可变光衰减器结构示意图。(a)整体;(b)核心部分细节

Fig. 1　Schematic diagram of structure of adjustable precision configurable variable optical attenuator. (a) Overall; (b) detail of core part

表 1　光纤与恒压泵的参数

Table 1　Parameters of fiber and constant pressure pumps

| Component | Parameter | Value |
|---|---|---|
| SMF-28 ultra single mode fiber | Wavelength /nm | 1260-1625 |
| | Fiber core diameter /μm | 8.2 |
| | Cladding diameter /μm | 125 |
| | Mode field diameter at 1550 nm /μm | 10.4 |
| Microfluidic OB1 MK3+ pressure controller | Stabilization time /ms | < 35 |
| | Pressure incremental adjustment accuracy /Pa | 1.22 |
| | Adjustment range /Pa | 0-20000 |

初始状态时,输出光纤与输入光纤对齐,可使光纤耦合效率最高。当流体注入方形槽内部储液结构后,薄膜受力凸起,带动光纤承载平台各层结构向上产生一定的位移,使得输入、输出光纤之间产生横向错位,耦合效率降低,造成光信号功率的衰减。光纤承载平台的移动量与容器内的流体压力呈一定的对应关系。通过精确控制恒压泵的压力输出,精准控制光纤承载平台的移动量,光衰减量可连续精准调节。相同压力下,VOA 薄膜厚度配置的不同会影响光纤位错精度,从而实现调节精度可配置。本文从仿真计算和实验角度研究不同配置的 VOA 光纤承载平台的移动量、光衰减量及薄膜配置对精度的影响。

## 3　VOA 驱动动力学和光学耦合效率仿真分析

位错型 VOA 涉及光纤的位错运动和光学分析,本文基于 COMSOL Multiphysics 软件和三维时域有限差分(FDTD)的方法,分别对 VOA 的驱动动力学行为和光学耦合效率进行仿真计算。

使用 COMSOL Multiphysics 软件进行优化结构参数与模拟状态分析,图 2(a)所示为简化设计的物理仿真模型。

流体从入口进入,设置薄膜为线弹性材料,在模型中求解用来描述流体流动的 Navier-Stokes 方程。流体 $\Delta\rho/\rho \ll 1$(其中 $\rho$ 为流体密度,$\Delta\rho$ 为流体内部的密度差),温度变化不明显,压缩性弱,马赫数远小于 1,所以可视为不可压缩的牛顿流体,则 Navier-Stokes 方程[24]可简化为

$$\nabla \cdot \boldsymbol{u} = 0, \tag{1}$$

$$\rho \frac{\partial \boldsymbol{u}}{\partial t} + \rho \cdot \boldsymbol{u} + \nabla(\boldsymbol{u}) = -\nabla p + \nabla \cdot \left[\mu\left(\nabla \boldsymbol{u} + \Delta \boldsymbol{u}^{\mathrm{T}}\right)\right] + \boldsymbol{F}, \tag{2}$$

式中:$\boldsymbol{u}$ 为流体速度;$p$ 是流体压力;T 代表转置;$\rho$ 为流体密度;$\mu$ 为流体黏度;$\boldsymbol{F}$ 为作用在流体上的外力。结构的变形根据弹性本构以及允许发生变形的几何非线性求解。流体从入口进入,对整个容器的槽内的各个结构壁受到黏性阻力和流体压力产生的作用力。设定流道内除了薄膜,其他的边界都为壁,并将薄膜添加到固体力学物理场,加入流固物理场进行耦合计算。薄膜承受流体施加的载荷为

$$\boldsymbol{F}' = -\boldsymbol{n} \cdot \left\{-p\boldsymbol{I} + \eta\left[\nabla \boldsymbol{u} + (\nabla \boldsymbol{u})^{\mathrm{T}}\right]\right\}, \tag{3}$$

式中:$\boldsymbol{n}$ 是边界的法向矢量;$\boldsymbol{I}$ 是单位矩阵;$F_T$ 是压力和黏性力的总和;$\eta$ 为流体的黏滞系数载荷。在 COMSOL Multiphysics 中基于任意拉格朗日-欧拉(ALE)方法求解在持续变形的几何域中的流体流动,并基于结构力学分析出的应变结果来计算新网格的坐标[25]。流固耦合的界面计算由 COMSOL Multiphysics

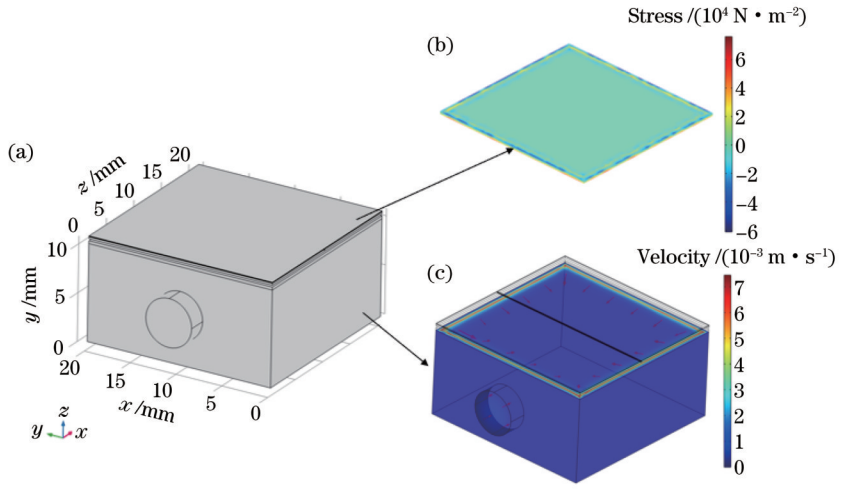


图 2　流-固耦合模拟区域。(a)模型图;(b)薄膜应力云图;(c)流体速度云图,结果来自 COMSOL Multiphysics 仿真软件(压力值为 488 Pa)

Fig. 2　Fluid-solid coupling simulation area. (a) Model diagram; (b) film stress nephogram; (c) nephogram of fluid velocity [results are obtained from COMSOL Multiphysics simulation software (pressure is 488 Pa)]

软件提供的接口处理,流体和固体的物理场移动网格遵循网格变形,这些条件[26]可表示为

$$\begin{cases} \boldsymbol{u}_{\mathrm{fluid}} = \boldsymbol{u}_{\mathrm{w}} \\ \boldsymbol{u}_{\mathrm{w}} = \dfrac{\partial \boldsymbol{u}_{\mathrm{solid}}}{\partial t},\ \boldsymbol{u}_{\mathrm{w}} \text{ is solution of fsi. vwall} \\ \sigma \cdot \boldsymbol{n} = \Gamma \cdot \boldsymbol{n},\ \Gamma = \left\{ -p\boldsymbol{I} + \eta\left[ \nabla \boldsymbol{u}_{\mathrm{fluid}} + (\nabla \boldsymbol{u}_{\mathrm{fluid}})^{\mathrm{T}} \right] \right\} \end{cases} \tag{4}$$

式中:$\boldsymbol{u}_{\mathrm{fluid}}$ 为流体速度矢量;$\boldsymbol{u}_{\mathrm{w}}$ 为流固耦合物理场接口参数;$\boldsymbol{u}_{\mathrm{solid}}$ 为固体位移速度矢量;$\sigma$ 为应力;$\boldsymbol{n}$ 为流固耦合边界的法向量;fsi. vwall 是 COMSOL Multiphysics 软件关于任意拉格朗日-欧拉方法流固耦合物理场的求解接口。通过式(1)~(4),可以计算出 $\boldsymbol{n}$ 与光纤承载平台上任一点的位移大小。如图 2(b)、(c)所示,流体、固体物理场耦合后,薄膜所受应力、容器内流体速度的大小均在四周沿边处分布均匀,控制流体压力,薄膜所受的力就会推动光纤承载平台垂直上升并稳定在一定的高度。

光纤横向位错光强耦合计算通常采用简化模型公式,利用时域有限差分的方法直接求解麦克斯韦方程组[27],计算 VOA 的光强耦合效率,所得结果将更准确[28]。VOA 的实验配置的参数为:光纤位错调节间隙为 20 nm,膜厚为 0.4 mm,所用激光波长为 1550 nm。

光衰减量的仿真计算结果如图 3 所示,这里取光衰减量约为 20 dB、40 dB、50 dB 时的三个点,即控制压力值为 366 Pa、439.2 Pa、1708 Pa,得到双光纤对接位错量与光纤纤芯内光能量的分布图。控制压力值从 0 到 439.2 Pa 时,即光衰减量约在 40 dB 以内时,光衰减量的增加明显很快,而控制压力值在 439.2 Pa 时,光衰减量增加趋势明显放缓。

## 4　实验结果与讨论

实验原理和装置实物如图 4(a)、(b)所示,其中光

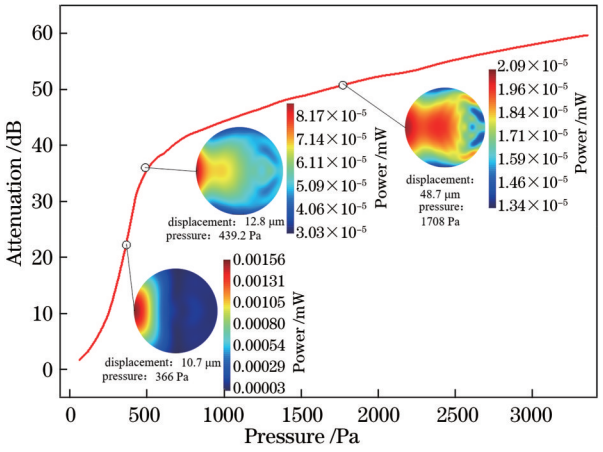


图 3　双光纤对接耦合效率与控制压力的关系,计算结果来自 FDTD 仿真软件($\lambda$=1550 nm)

Fig. 3　Dual fiber docking coupling efficiency varying with control pressure [results are from FDTD simulation software ($\lambda$=1550 nm)]

纤调整架用来辅助精准对齐胶合输入、输出光纤及测量测试光纤承载平台移动量。所设计的 VOA 装置可动部件和固定输出光纤的 V 型槽分别固定于光纤调整架右侧、左侧,控制流体入口接恒压泵的通道接口。输入、输出光纤分别与可调谐激光器和光功率计相连。调节光纤调整架对准输入、输出光纤,并预留 20 nm 的位错调节间隙。设置恒压泵的压力调节间隔为 61 Pa(最小压力调节精度的 50 倍),PDMS 薄膜厚度为 0.4 mm,测试光纤承载平台移动量与压力的关系,如图 5 所示,考虑到光衰减器的值为 40 dB,最大压力取值略大于光衰减器的 9 倍,即 549 Pa。

图 5(a)中,控制压力从 61 Pa 升至 549 Pa 过程中,光纤承载平台的移动量与控制压力呈线性关系,压力每增加 61 Pa,平台位移量增量为 1.75 μm,光衰减量

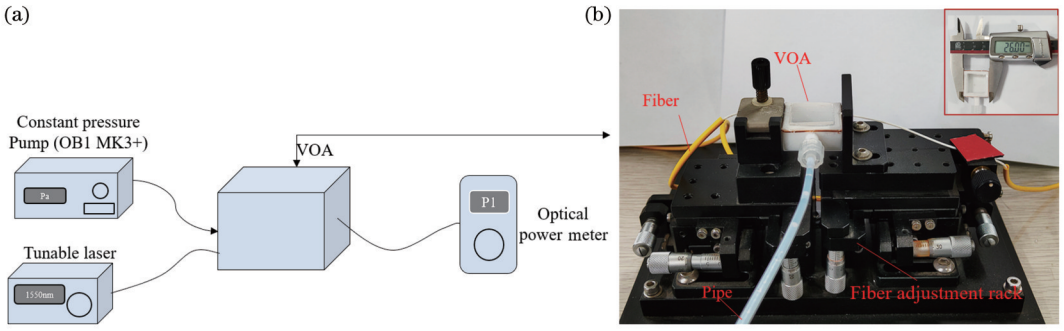


图 4　光强耦合效率实验原理和实物测试装置。(a)实验原理;(b)实物测试装置

Fig. 4　Experimental principle and physical test device of light intensity coupling efficiency. (a) Experimental principle; (b) physical test device

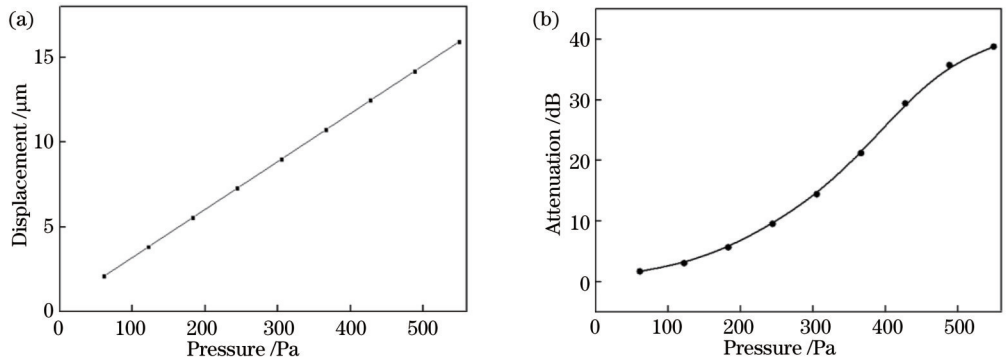


图 5　光纤承载平台移动量、光衰减量与压力的关系(薄膜厚度为 0.4 mm)。(a)承载平台移动量与压力的关系;(b)光衰减量与压力的关系

Fig. 5　Relationship among fiber bearing platform movement, optical attenuation, and pressure (film thickness is 0.4 mm). (a) Fiber bearing platform movement varying with pressure; (b) optical attenuation varying with pressure

与压力的关系呈近似二次曲线,如图 5(b)所示。

基于图 6(a)所示的原理图,采用 GLSUN 公司的插损回损仪和桂林 UC 公司的可调谐宽带调谐激光源进行插入损耗、回波损耗及波长相关损耗的测量。实验测得插入损耗为 1.24 dB,回波损耗为 −54 dB。在可调激光光源下测量范围内的光衰减值为 10 dB、20 dB、30 dB、40 dB 时,波长相关损耗分别为 0.06 dB、0.24 dB、0.59 dB、0.89 dB,波长相关损耗均小于 1 dB,如图 6(b)所示。取 1550 nm 波长进行重复性实验,所得结果较好。器件的响应时间包括液压驱动响应时间和光纤移动时间两部分,其中液压驱动响应时间为表 1 所示的 35 ms,而光纤固定于 V 型槽,不存在振动,故光纤移动时间远小于液压控制时间,由此估算得到整个 VOA 的响应时间小于 50 ms。

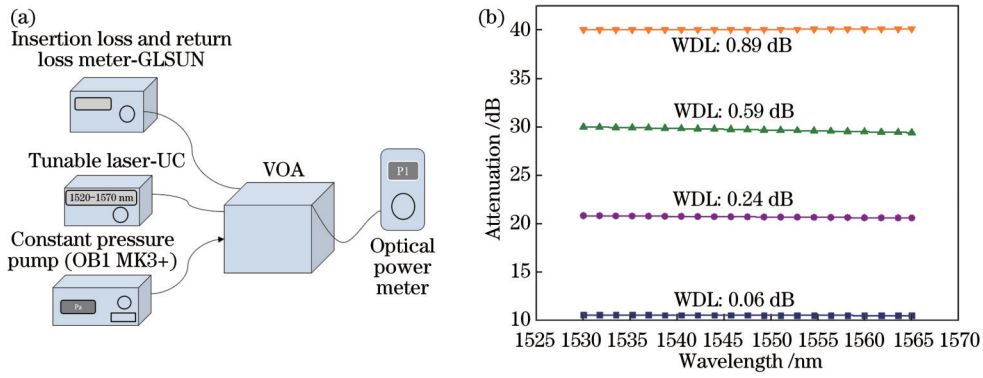


图 6　实验测量。(a) 原理图;(b) 波长相关损耗(1530~1565 nm)

Fig. 6　Experimental measurement. (a) Schematic; (b) wavelength dependent loss (1530-1565 nm)

为研究不同膜厚对配置 VOA 的调节精度的影响,薄膜厚度设置为 0.3 mm、0.4 mm、0.5 mm,压力间隔为 12.2 Pa,测量 VOA 的精度,实验结果如图 7 所示,对实验关系曲线进行拟合并求导得到斜率,进而确

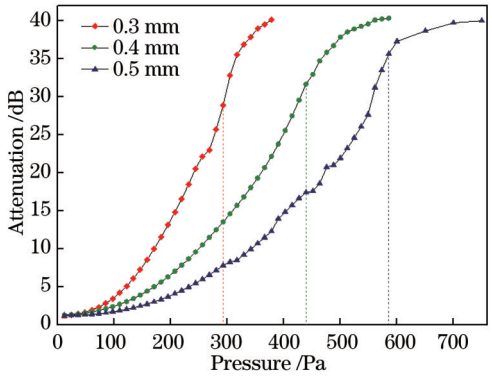


图 7　不同膜厚 VOA 的光衰减量与控制压力的关系

Fig. 7　Light attenuation varying with control pressure for VOA configured with different film thicknesses

定调节精度。图 7 中三条曲线在加压较小时斜率较小，调节精度较高，随着加压增加，关系曲线斜率迅速增加。例如：设定 VOA 动态范围为 10 dB 时，膜厚为 0.3 mm、0.4 mm、0.5 mm 的 VOA 的最低调节精度分别为 0.12 dB、0.06 dB、0.04 dB。设定 VOA 的动态范围等于或大于 40 dB 时，曲线斜率变化存在拐点，此时 VOA 的最低调节精度可在拐点附近分别取为 0.16 dB、0.15 dB、0.11 dB。

## 5　结　　论

提出了一种调节精度可配置的位错型可调光衰减器，通过驱动薄膜弹起光纤发生横向位移，实现对接光纤横向位错及光学衰减。仿真分析与实验测量均表明，本可变光衰减器的插入损耗为 1.24 dB，回波损耗为 −54 dB，波长相关损耗小于 1 dB，动态范围可达 60 dB。本器件的薄膜厚度能影响调节精度，调节精度与膜厚的关系可由光衰减量曲线拟合求得。当设定可变光衰减器的光衰减动态范围分别为 10 dB 和 40 dB 时，对于配置 0.5 mm 厚度的薄膜，其调节精度可分别优于 0.04 dB 和 0.11 dB。本装置可将流体压力/压强的调节转化为光纤横向微位移精密控制，为光纤类产品的研制提供一个新思路。

### 参　考　文　献


[1] Lee C K. Arrayed variable optical attenuator using retro-reflective MEMS mirrors[J]. IEEE Photonics Technology Letters, 2005, 17(12): 2640-2642.

[2] Unamuno A, Blue R, Uttamchandani D. Modeling and characterization of a vernier latching MEMS variable optical attenuator[J]. Journal of Microelectromechanical Systems, 2013, 22(5): 1229-1241.

[3] Llobera A, Villanueva G, Cadarso V J, et al. Polymeric MOEMS variable optical attenuator[J]. IEEE Photonics Technology Letters, 2006, 18(22): 2425-2427.

[4] Umezawa H, Kato T. Variable magneto-optical devices for fiber-optic communication systems[J]. Transactions of the Magnetics Society of Japan, 2004, 4: 330-333.

[5] Hah D. Linear variable optical attenuators with shaped-finger comb-drive actuators[J]. Applied Optics, 2020, 59(2): 277-284.

[6] Dai X H, Zhao X L, Ding G F, et al. Electromagnetic MEMs eight-channel variable optical attenuator array[J]. Proceedings of SPIE, 2004, 5641: 1-6.

[7] Hah D. Planar MEMS variable optical attenuators (VOAs) with linear attenuation-voltage characteristics[C]//2019 Symposium on Design, Test, Integration & Packaging of MEMS and MOEMS (DTIP), May 12-15, 2019, Paris, France. New York: IEEE Press, 2019.

[8] Bashir A, Katila P, Ogier N, et al. A MEMS-based VOA with very low PDL[J]. IEEE Photonics Technology Letters, 2004, 16(4): 1047-1049.

[9] Panchal R, Sinha A. Low threshold optical attenuator based on electrically tunable liquid crystal cladding waveguide[J]. Optics Communications, 2022, 513: 128089.

[10] Mane S M, Digge J, Rindhe B. Performance analysis of variable optical attenuator on different materials[C]//2021 6th International Conference for Convergence in Technology (I2CT), April 2-4, 2021, Maharashtra, India. New York: IEEE Press, 2021.

[11] Kim Y Y, Yun S S, Park C S, et al. Refractive variable optical attenuator fabricated by silicon deep reactive ion etching[J]. IEEE Photonics Technology Letters, 2004, 16(2): 485-487.

[12] 陈之厦, 梁斌明, 庄松林. 基于二维光子晶体的温控光衰减器[J]. 激光与光电子学进展, 2019, 56(15): 152301.
Chen Z X, Liang B M, Zhuang S L. Temperature-controlled optical attenuator based on two-dimensional photonic crystals[J]. Laser & Optoelectronics Progress, 2019, 56(15): 152301.

[13] Andreev D P, Andreeva E I. Fiber optic attenuator[J]. Journal of Physics: Conference Series, 2021, 2086(1): 012128.

[14] Morozov V, Fan H, Eldada L, et al. Fused fiber optic variable attenuator[C]//Optical Fiber Communication Conference. Technical Digest Postconference Edition. Trends in Optics and Photonics Vol. 37 (IEEECat. No. 00CH37079), March 7-10, 2000, Baltimore, MD, USA. New York: IEEE Press, 2000: 22-24.

[15] 谢晓强, 戴旭涵, 赵小林, 等. 位错型微机械可变光衰减器的研究[J]. 光学学报, 2005, 25(5): 717-718.
Xie X Q, Dai X H, Zhao X L, et al. Research on an offset-type micro mechanical variable optical attenuator[J]. Acta Optica Sinica, 2005, 25(5): 717-718.

[16] Li Q, Au A A, Lin C H, et al. An efficient all-fiber variable optical attenuator via acoustooptic mode coupling[J]. IEEE Photonics Technology Letters, 2002, 14(11): 1563-1565.

[17] 崔宇龙, 周智越, 黄威, 等. 中红外光纤激光技术研究进展与展望[J]. 光学学报, 2022, 42(9): 0900001.
Cui Y L, Zhou Z Y, Huang W, et al. Progress and prospect of mid-infrared fiber laser technology[J]. Acta Optica Sinica, 2022, 42(9): 0900001.

[18] 董富宁, 杨庆, 罗曼丹, 等. 一种基于磁致伸缩效应和光纤光栅的电流传感器[J]. 光学学报, 2022, 42(8): 0806001.
Dong F N, Yang Q, Luo M D, et al. Current sensor based on magnetostriction and fiber Bragg grating[J]. Acta Optica Sinica, 2022, 42(8): 0806001.

[19] 李敏, 丛爱民, 曹万苍, 等. 基于级联聚合物腔的光纤温度和磁场传感探头[J]. 中国激光, 2022, 49(9): 0906004.
Li M, Cong A M, Cao W C, et al. Temperature and magnetic field fiber sensing probe based on cascaded polymer cavities[J]. Chinese Journal of Lasers, 2022, 49(9): 0906004.

[20] 徐廷廷, 杨玉强, 杨文龙, 等. 基于 PDMS 膜封装空芯光纤的级联双腔温度传感器[J]. 光学学报, 2022, 42(8): 0806004.
Xu T T, Yang Y Q, Yang W L, et al. Cascaded double-cavity temperature sensor based on hollow fibers encapsulated by PDMS membrane[J]. Acta Optica Sinica, 2022, 42(8): 0806004.

[21] 黄旭光, 叶晓靖, 张小康, 等. 光纤型热光可调光衰减器的设计及其衰减分析[J]. 光学学报, 2006, 26(12): 1787-1791.
Huang X G, Ye X J, Zhang X K, et al. Design and attenuation analysis for fiber-typed variable optical attenuator based on

thermo-optic effect[J]. Acta Optica Sinica, 2006, 26(12): 1787-1791.
[22] Duduś A N, Blue R, Zagnoni M, et al. Theoretical and experimental analysis of side-polished fiber optofluidic variable attenuator[C]//2014 International Conference on Optical MEMS and Nanophotonics, August 17-21, 2014, Glasgow, UK. New York: IEEE Press, 2014: 67-68.
[23] 郝永芹. 光纤定位硅V型槽的设计与制作[D]. 长春: 长春理工大学, 2002.
Hao Y Q. The design and fabrication of silicon V-groove arrays [D]. Changchun: Changchun University of Science and Technology, 2002.
[24] Grzybowski H, Mosdorf R. Modelling of two-phase flow in a minichannel using level-set method[J]. Journal of Physics: Conference Series, 2014, 530: 012049.
[25] Weddemann A, Thümmler V. Stability analysis of ALE-methods for advection-diffusion problems[EB/OL]. [2021-04-05]. https://cn. comsol. com/paper/stability-analysis-of-ale-methods-for-advection-diffusion-problems-4887.
[26] Elabbasi N, Bergstrom J, Brown S. Fluid-structure interaction analysis of a peristaltic pump[EB/OL]. [2021-05-04]. https://www.comsol.ru/paper/download/84013/elabbasi_paper.pdf.
[27] Salski B, Celuch M, Gwarek W. FDTD for nanoscale and optical problems[J]. IEEE Microwave Magazine, 2010, 11(2): 50-59.
[28] Joseph R M, Taflove A. FDTD Maxwell's equations models for nonlinear electrodynamics and optics[J]. IEEE Transactions on Antennas and Propagation, 1997, 45(3): 364-374.

# Variable Optical Attenuator with Configurable Adjustment Accuracy

Wei Shuo, Chen Tao*, Chen Jing, Kong Meimei, Guan Jianfei

*College of Electronic and Optical Engineering & College of Flexible Electronics (Future Technology), Nanjing University of Posts and Telecommunications, Nanjing* 210000, *Jiangsu, China*

## Abstract

**Objective** A variable optical attenuator is a key component for wavelength division multiplexing (WDM) transmission node power equalization, optical amplifier gain flattening, multiplexing point channel balancing, and receiving node power management in fiber optic communication. A fiber optic type variable optical attenuator has the advantages of simple structure, low insertion loss, low cost, and easy to interface with other optical fibers and waveguide structure, and is widely used. The adjustment accuracy and attenuation range are very important parameters of the variable optical attenuator, and there are few products with high adjustment accuracy and large attenuation range. In this paper, based on the traditional dislocation-type optical fiber variable optical attenuator with large dynamic range, the fluid pressure/pressure regulation is transformed into optical fiber micro-displacement control, which is easy to realize the micro-displacement precision control of optical fiber products to replace the high cost precision mechanical adjustment instrument of such products. In addition, the device meets the requirements of optical networks for attenuators, can work in a wide range of attenuation, and has low insertion loss and low wavelength-dependent loss, as well as compact structure, low cost, and high accuracy. According to the VOA optical power adjustment curve, film thickness can be selected to achieve configurable VOA optical attenuation accuracy.

**Methods** The designed variable optical attenuator device is fabricated by ultra-precision processing technology. It contains components such as the polydimethylsiloxane (PDMS) elastic film, optical fiber carrying platform, and constant pressure pump. The adjustment of fluid pressure is transformed into micro-displacement control of the optical fiber by driving the ejection of the film through the fluid constant pressure pump, thus realizing the lateral dislocation of the docking fiber, and the optical attenuation is realized based on the dislocation of the ejected film driven by the fluid constant pressure pump and the docking fiber, while the adjustable accuracy of the optical intensity coupling efficiency is achieved by selecting the appropriate film thickness. We use the COMSOL Multiphysics software and three-dimensional finite difference time domain (FDTD) method to simulate and calculate the driving kinetic behavior and optical coupling efficiency of VOA, respectively. And in the experimental measurement stage, by replacing the film thickness of the device and adjusting the input pressure of the constant pressure pump, the trace mechanical dislocation and optical attenuation data are measured and the coupling efficiency is calculated, and then the relationship among the movement of the fiber-bearing platform, optical attenuation, and pressure control, and relationship between the wavelength-dependent loss and the optical attenuation of VOA with different film thickness and control pressure are derived. Finally, the relationship between the configuration of the film thickness and the precision of the variable optical attenuator is fitted numerically.

**Results and Discussions** The experimental results show that the variable attenuation range of this attenuator is greater than 60 dB (Fig. 3) with an insertion loss of 1.24 dB (Fig. 5) and a wavelength-dependent loss less than 1 dB (Fig. 6) under appropriate film thickness conditions. The variable optical attenuator is used for repeatability experiments at the

wavelength of 1550 nm with satisfied performance. The response time of the device is less than 50 ms. In order to study the influence of film thicknesses on the regulation accuracy of the configured VOA, the film thicknesses are set to 0.3 mm, 0.4 mm, and 0.5 mm, and the pressure interval is 12.2 Pa. The accuracy of the VOA is measured, and the worst regulation accuracy of the VOA with film thicknesses of 0.3 mm, 0.4 mm, and 0.5 mm can be obtained when the dynamic range of the VOA is 10 dB. When the dynamic range of VOA is set equal to or greater than 40 dB, there is an inflection point for the change of the slope of the curve, and the worst adjustment accuracy of VOA can be taken as 0.16 dB, 0.15 dB, and 0.11 dB respectively near the inflection point. When the dynamic optical attenuation range of the variable optical attenuator is set to 10 dB and 40 dB, the adjustment accuracy is better than 0.04 dB and 0.11 dB for a film thickness of 0.5 mm, respectively (Fig. 7). The tuning accuracy will be higher when the film thickness increases.

**Conclusions** A variable optical attenuator with configurable adjustment accuracy is proposed to achieve transverse dislocation and optical attenuation of docked optical fibers by driving the film to pop up the fiber for lateral displacement. Both the numerical analysis and experimental measurement results show that the variable optical attenuator has an insertion loss of 1.24 dB, a return loss of −54 dB, a wavelength dependent loss of less than 1 dB, and a dynamic range of 60 dB. The thickness of the film of the device can affect the adjustment accuracy, and the relationship between the adjustment accuracy and the film thickness can be obtained by fitting the optical attenuation curve. This device can transform the adjustment of fluid pressure/pressure into precise control of transverse micro-displacement of fiber, which provides a new idea for the development of fiber optic products.

**Key words** optical communications; variable optical attenuator; lateral dislocation; film drive; configurable accuracy